Case Studies in Thermal Engineering 34 (2022) 102016

Contents lists available at ScienceDirect

Case Studies in Thermal Engineering

journal homepage: www.elsevier.com/locate/csite

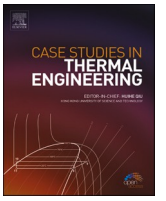

Investigation on inlet obstruction in transitional flow regime: Heat transfer augmentation and pressure drop analysis

Basma Souayeh [a,b,*], Suvanjan Bhattacharyya [c], Najib Hdhiri [b], Mir Waqas Alam [a], Essam Yasin [d], Muhammad Aamir [e]

[a] Department of Physics, College of Science, King Faisal University, PO Box 400, Al-Ahsa, 31982, Saudi Arabia
[b] Department of Physics, Laboratory of Fluid Mechanics, Faculty of Sciences of Tunis, University of Tunis El Manar, 2092, Tunis, Tunisia
[c] Department of Mechanical Engineering, Birla Institute of Technology and Science Pilani, Pilani Campus, Vidya Vihar, Pilani, 333 031, Rajasthan, India
[d] Department of Mathematics, Statistics and Physics, College of Arts and Sciences, Qatar University, 2713, Doha, Qatar
[e] Department of Basic Science, Preparatory Year Deanship, King Faisal University, Al Hofuf, Al-Ahsa, 31982, Saudi Arabia

ARTICLE INFO

Keywords:
Transition flow regime
Ribbed prism
Thermohydraulic
Heat transfer
Friction factor

ABSTRACT

Thermohydraulic characteristics of air as the working medium in a circular heated channel fitted with inlet obstruction (ribbed prism) at the inlet is carried out experimentally for transitional flow regime. The ribbed prism is fabricated using aluminum metal. Three non-dimensional parameters clearance ratio (C = 0.4, 0.5 and 0.6) and pitch ratio (e = 0.12, 0.15 and 0.16) were investigated. The Reynolds number (Nu) varied from 500 to 7036 to cover all the flow regimes. Experiments were conducted at two constant heat fluxes of 0.5 kW/m^2 and 1 kW/m^2. It was found that start and end of transitional flow regime was influenced by insertion of the inlet obstruction at the inlet of the test section. With placement of prism in the channel, the boundaries of transition changes when compared with the plain channel. It is observed that transition starts early and also end early to the transition limit of plain channel. Heat flux shows significant influence on the onset and termination of the transition. At higher heat flux the transition starts later and terminates later when compared with the lower heat flux conditions. For the case of C = 0.6 and e = 0.16, the transition begins Re = 1648 and ends at Re = 3387 for 1 kw/m^2 heat flux. The transition of 0.5 kW/m^2 of heat flux for C = 0.6 and e = 0.16 begins at Re = 1554 and ends at Re = 3321. Correlations were also developed for predicting the Nusselt number and friction factor and the results are useful to design solar thermal systems and heat exchangers.

1. Introduction

In past two decades, the energy consumption across the world grows by several folds. This is due to the drastic development observed in all sectors of industries. The advancement in the technology enables all sections of the society to enjoys it perk. But this advancement in the technology pushed the limits for depleting non-renewable energy sources. Several reforms internationally have been introduced in the previous years to conserve the non-renewable energy sources. These reforms bring new zenith in the field of renewable energy especially solar energy. A race is going on amongst the economies of world to reduce their reliability on the non-renewable sources by harnessing the maximum among of solar energy. Solar energy is harness with the help of solar absorber

* Corresponding author. Department of Physics, College of Science, King Faisal University, PO Box 400, Al-Ahsa, 31982, Saudi Arabia.
E-mail addresses: bsouayeh@kfu.edu.sa, basma.souayeh@gmail.com (B. Souayeh).

https://doi.org/10.1016/j.csite.2022.102016
Received 31 January 2022; Received in revised form 21 March 2022; Accepted 5 April 2022
Available online 13 April 2022

plates, solar concentrators, solar collectors, etc. A heat exchanger (HE) is used to exchange this energy extracted from sun with some different fluid to utilize it further. Several research are going on to reduce the size and volume of such devices with enhanced performance. Even, efforts are also made at the nanoscale level [1].

Heat exchangers are most widely used equipment in power generation, automobile, defense, aviation, chemical, medical and pharmaceutical industries [2–4]. Heat exchangers play an important role in transfer of energy from one fluid to another [5–8]. Hence, it is desirable to design and develop a heat exchanger which serves out the purpose with maximum efficiency and effectiveness. Heat exchangers generally design to works in laminar and turbulent flow regime. However, it has been observed previously by some researchers that sometimes heat exchanger also operates in the transitional flow regime (TFR).

The credit of initial investigations in the field of TFR goes to Ghajar and group [9–14]. Main objective behind the investigation was to gather the data for heat transfer and friction factor this flow regime to understand the fluid behaviour. Studies in TFR are still in the early stage on very few manuscripts available in the open literature specially dedicated to the thermohydraulic performance in TFR.

Ghajar and co-workers [9,10,15–17] carried out experimental investigations for heat transfer and pressure drop in TFR with three inlet geometries namely, Re-entrant, square-edge and bell mouth inlet. Besides, influences of developing or developed flow, and heat flux on the TFR were reported. It was found that smoother the inlet, late the transition begins and later it ends. While blunt inlets

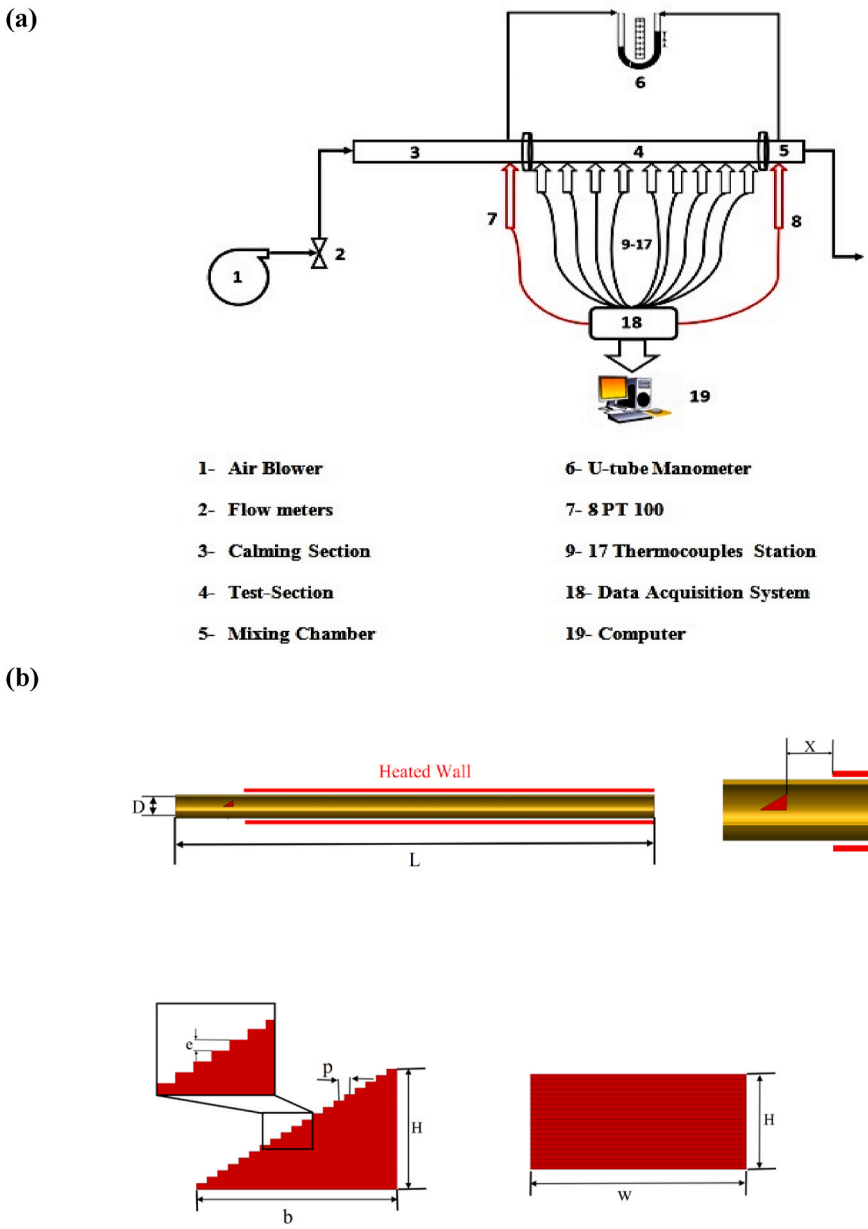

Fig. 1. (a) Schematic of Experimental test rig, and (b) circular tube with inlet obstruction (triangular ribbed prism).

started and ends the transition earlier. Also, it was also reported that increase in heat flux further delayed the onset and end of the transition. Water-Ethylene Glycol mixture in different concentrations was used for the investigations. It was reported from these studies that transition may have started around Reynolds number of 600 and can goes up to the Reynolds number of 10000. The investigations of Ghajar and co-workers change the concept of laminar-transition-turbulent flow regimes. The experimental data of their work reflects the variation in TFR with changes in the inlet geometries, operating conditions, etc.

Moving on the same track, Meyer and Co-workers [6–13] also carried out series of experiments with different inlet geometries, enhanced tubes, turbulators, working fluids (water and nanofluids). Besides, they also experimented by changing the orientation of test section from horizontal to vertical [18]. While the research work of Ghajar and co-workers mainly concentrated on the plain channels with different inlet geometries, Meyer and Co-workers explored by employing various modifications as mentioned above. The research work did by Meyer and co-workers provide a new dimension to this young research field. The results obtained by them are very interesting and correlations developed by them are wildly accepted by the scientific community very well.

2. Objective of current investigation

After thoroughly reviewing the various articles related to the field, authors of this paper come to the point that only few manuscripts are available which are related to channel modifications which includes works of Meyer and Olivier [19,20] and Abolarin et al. [21–23]. While Meyer and Olivier work on the enhanced channel [19,20], Abolarin et al. [21–23] investigated the influence of turbulators (Conventional twisted tapes, clockwise and anticlockwise twisted tapes, and peripheral cut twisted tape with ring inserts) on the TFR. This provides a research gap for further exploration in this field. It is noted from the previous work that no work has been reported so far on the influence of inlet obstruction on the thermohydraulic behaviour in the TFR. Hence, seeking this as a positive opportunity, authors of this work carried out experimental investigation in a channel with ribbed prism bluff body placed at the inlet of the channel to study the thermohydraulic performance of the working fluid in transitional flow. For present experimental investigation, air is used as the working fluid with Reynolds number varied from 500 to 7036 to cover all the three flow regimes. Also the considered flow regime helps in understanding the variation in the output amongst three flow regimes.

3. Experimental setup, procedure and uncertainity analysis

Experimental test rig (Refer Fig. 1(a)) consists of air blower having capacity of 7 kW. Fresh air at atmospheric temperature and pressure sucked in through the air blower and passes through the flow meters which measures the flow rate of the air. A control valve is provided before the flow meter to control the flow rate. Air then passes through the calming section. Calming section is made of hollow metallic cylindrical duct having diameter of 30 mm and is 1500 mm long. The calming section brings the uniformity and steadiness to the flow velocity. Calming section is connected to the test section with the help of flange. Test section is made of brass having diameter (D) of 20 mm and length (L_2) of 2000 mm. The total length (L) of the tube is 2500 mm and the non-heated portion length (L_1) is 500 mm. The obstruction (ribbed prism) is place at a distance (X) of 100 mm from the entry of the tube section as shown in Fig. 1 (b). Two temperature probe PT 100 are connected at the inlet and outlet of the test section to measure the bulk temperature of in and out air. Besides, 36 T-type thermocouples are also attached to the test section to measure the temperature of the surface of the test section at different position. Four thermocouples are attached at one station at an angle of 90° from each other. Average of these four thermocouples reading will give the reading of surface temperature at a station. Total nine such stations at different length are used to measure the temperature of test section surface. Thermocouples are brazed on the surface of test section. Two high-quality porcelain nichrome heaters are also coiled around the test section and are attached with the variac to control the voltage. All the 36 thermocouples and 2 PT 100 are connected to the data acquisition system which is connected to the computer to collect the temperature reading at a regular interval of 1 s. A u-tube manometer is also attached between inlet and outlet of the test section to measure the pressure drop across the channel. The whole test rig is insulated with the layers of insulation tape made up of mica, glass wool and jute followed by a layer of glass wool then jute bag and finally microfiber sheet. The purpose of insulation is to minimize the heat loss to the atmosphere.

It takes around 1–1.5 h to achieve the steady state depending upon the flow rate and heat flux. Steady state is assumed to be reached once no major fluctuation in temperature, flow rate and pressure drop were observed. Initially, all the valves were kept fully opened and then were gradually closed depending upon the desired flow rate. To reduce the flow fluctuation, bypass valve was continuously adjusted. Heat flux to the test section is adjusted with the help of variac. Once all the setting is done and steady state is assumed, reading will be recorded to the data acquisition system. The average of data points collected will collectively result in a single reading. The above procedure was repeated to for different flow rate.

All the equipment used in the experiments are calibrated and uncertainty analysis is carried out to determine the percentage error

Table 1
Range of equipment used in Test rig.

Equipment	Range
Blower	7 kW
Rotameter	1.0–120 LPH
U-tube manometer	0.0–150 mm of Hg
Variac	0–270 V
Thermocouples	−373 to 623 K

in the measurement. The principles suggested by Dunn [24] in their book were assessed to determine the uncertainty at 95% confidence level. Thermocouples and PT 100 calibrated using a reference thermometer within an accuracy of ± 0.04 °C. The uncertainty in estimating Reynolds number was 3.5%, and that of friction factors was 4%, while the uncertainty in estimating the Nusselt number was within 6%. Table 1 shows the measuring range of various equipment while Table 2 shows uncertainty of various parameters.

4. Data reduction

Following parameters has been used in the present investigation (refer Fig. 1(b)):

Diameter (D), mm	20
Tube length (L), mm	2500
Non-heated tube length (L_1), mm	500
Heated tube length (L_2), mm	2000
Pitch ratio (e = E/H)	0.12, 0.15 and 0.16
Heat flux, (q), kW/m^2	0.5 and 1.0
Clearance ratio (C = H/D)	0.4, 0.5 and 0.6

The following set of equations are utilized for the calculation purpose:
Heat transferred to the air is given by Ref. [2]:

$$Q_{Air} = m^{'} * C_p (T_{Out} - T_{in}) \tag{1}$$

Heat Flux is given by Ref. [25]:

$$q = Q_{Air}/A_{Sur} = Q_{Air}/\pi DL \tag{2}$$

Reynolds number (*Re*) will be calculated using the following relation [26]:

$$Re = 4 * m^{'}/\pi D\mu \tag{3}$$

For determination of local temperature at various position [23]:

$$T(x) = T_{in} + (T_{out} - T_{in})x/L \tag{4}$$

For the calculation of bulk temperature [2]:

$$T_b = T_{in} + T_{out}/2 \tag{5}$$

The local convective heat transfer coefficient can be calculated as [25]:

$$h(x) = q/T_{sx} - T_x \tag{6}$$

Where T_{sx} is mean surface temperature at position x and T_x is the mean temperature of working fluid at position x.
For calculating the average heat transfer coefficient [27]:

$$h = q/T_s - T_b \tag{7}$$

Where T_s is the surface temperature.
The Nusselt number (*Nu*) is given by Ref. [25]:

$$Nu = hD/k \tag{8}$$

The heat transfer can also be represented using the Colburn j-factor or simply called j-factor is given by Ref. [25]:

$$j = Nu/RePr^{\frac{1}{3}} \tag{9}$$

For friction factor calculation, the formula is [28]:

Table 2
Uncertainty of various parameters.

Variables	Error (%)
Velocity	0.184
Voltage of Heater	0.146
Resistance	0.38
Power supplied to heater	0.171
Current	0.226
Ambient temperature	0.120

$$f = \frac{\Delta p}{\frac{L}{D}\frac{1}{2}\rho V^2} \tag{10}$$

For calculating the thermal performance factor, the following formula can be used [2,29]:

$$\eta = \frac{Nu/Nu_0}{(f/f_0)^{0.33}} \tag{11}$$

Where the subscript 0 is used to denote the plain duct.

5. Validation of the results

Fig. 2 (a) and 2 (b) depicts the validation of Nusselt number and friction factor against the Reynolds number respectively. For validation of Nusselt number and friction factor in plain channel in laminar flow regime, well renowned correlations of Nu = 4.36 and Poiseuille were employed, respectively. And for the validation in turbulent flow regime, correlations of Meyer et al. and Blasius were employed for Nusselt number and friction factor, respectively. For Nusselt number validation, the average deviation of 3.4% is reported while for the friction factor the deviation is only 0.5%. In laminar flow regime, the Nusselt number started deviating (increases with Reynolds number) from the value of Nu = 4.36 after Re = 600. This is due to the dependence of Nusselt number on the Reynolds number [27]. Based on the percentage deviation between experimental and predicted data using the correlations, it can be said that a very good agreement is observed.

Fig. 2 (c) depicts the Colburn j-factor for plain channel. For depicting the critical Reynolds number of beginning and end of the transition regime, line fitting method is used. The line L-L shows the fitting line for laminar flow regime, Y–Y represents the transition regime and T-T shows the turbulent flow regime. The intersection of L-L line and Y–Y lines gives the critical Reynolds number for onset of transition while the intersection point of line Y–Y and T-T gives the critical Reynolds number for end of transition. On analysis the data, it was found that critical Reynolds number for onset of transition is Re = 2562 and for end of transition is Re = 3802. This brings the transition width of Re = 1240.

6. Results and discussion

6.1. Nusselt Number (Nu)

Under the same conditions, the Nusselt number is defined as the ratio of convection heat transfer to fluid conduction heat transfer. Fig. 3 (a, b and c) shows the variation of Nusselt number with Reynolds number.

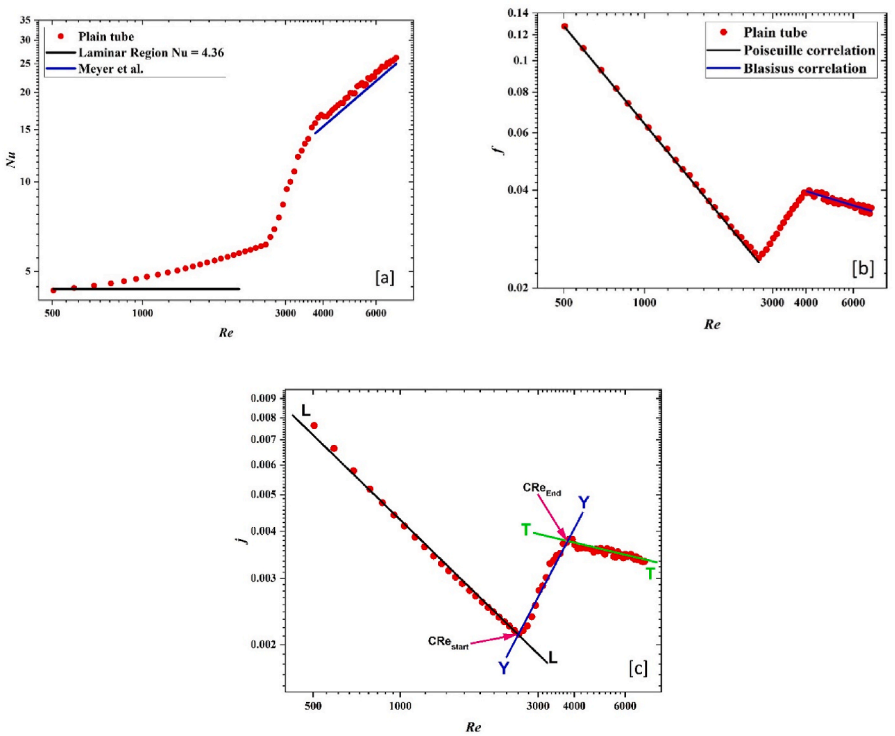

Fig. 2. (a) Validation of Nusselt Number, (b) Validation of Friction factor, and (c) *j*-factor as function of Re for plain tube.

Fig. 3 (a) shows Nusselt number variation for constant pitch ratio (e = 0.16) and variable clearance ratio (C = 0.4, 0.5 and 0.6) for constant heat flux (q = 1 kW/m^2). Following inference can be made by observing the graph:

(i) Enhancement in heat transfer is observed when results were compared with plain channel.
(ii) Highest enhancement in Nusselt number were reported for C = 0.6 and e = 0.16 while lowest enhancement was reported for C = 0.4 and e = 0.16 for channel having ribbed prism inserted.
(iii) The presence of ribbed prism in the flow line results in the earlier transition. This is due to the disturbance in the flow field which results in the early transition.
(iv) For C = 0.4 and e = 0.16, the transition begins at Re = 2121 and ends at Re = 4529. For C = 0.5 and e = 0.16, the transition begins at Re = 1750 and ends at Re = 3769. For C = 0.6 and e = 0.16, the transition begins at Re = 1648 and ends at Re = 3387.

Fig. 3 (b) shows the Nusselt variation for variable pitch ratio (e = 0.12, 0.15 and 0.16) and constant clearance ratio (C = 0.6) for constant heat flux (q = 1 kW/m^2). The inference made by observing the graphs are as follows:

(i) Highest enhancement in Nusselt number was reported for C = 0.6 and e = 0.16 while lowest enhancement was reported for C = 0.6 and e = 0.12 for channel having ribbed prism.
(ii) For lower pitch ratio, the gap between the ribs is large. This results in lesser mixing of fluids and hence the lower Nusselt value.
(iii) On comparison earliest beginning and end of transition was reported for C = 0.6 and e = 0.16. For the given case the transition begins at Re = 1648 and ends at Re = 3387. For C = 0.6 and e = 0.15, the transition begins at Re = 1655 and ends at Re = 3412. And For C = 0.6 and e = 0.12, the transition begins at Re = 1646 and ends at Re = 3502.

Fig. 3 (c) shows the variation of Nusselt number for C = 0.6 and e = 0.16, for heat flux 0.5 and 1 kW/m^2. It is clear from the plot that increase in heat flux results in higher Nusselt number. It is also worth noticing that for higher heat flux value the transition begins later when compared with the lower heat flux results. As the heat flux increases, the randomness in the air particles increases. This increases the viscosity of the air. This results in the delayed transition at higher heat flux. The transition of 0.5 kW/m^2 of heat flux for C = 0.6 and e = 0.16 begins at Re = 1554 and ends at Re = 3321.

6.2. Friction factor (f)

Friction factor depicts the resistance offered to the working medium in the fluid domain. Fig. 4 (a, b, and c) depicts the variation in

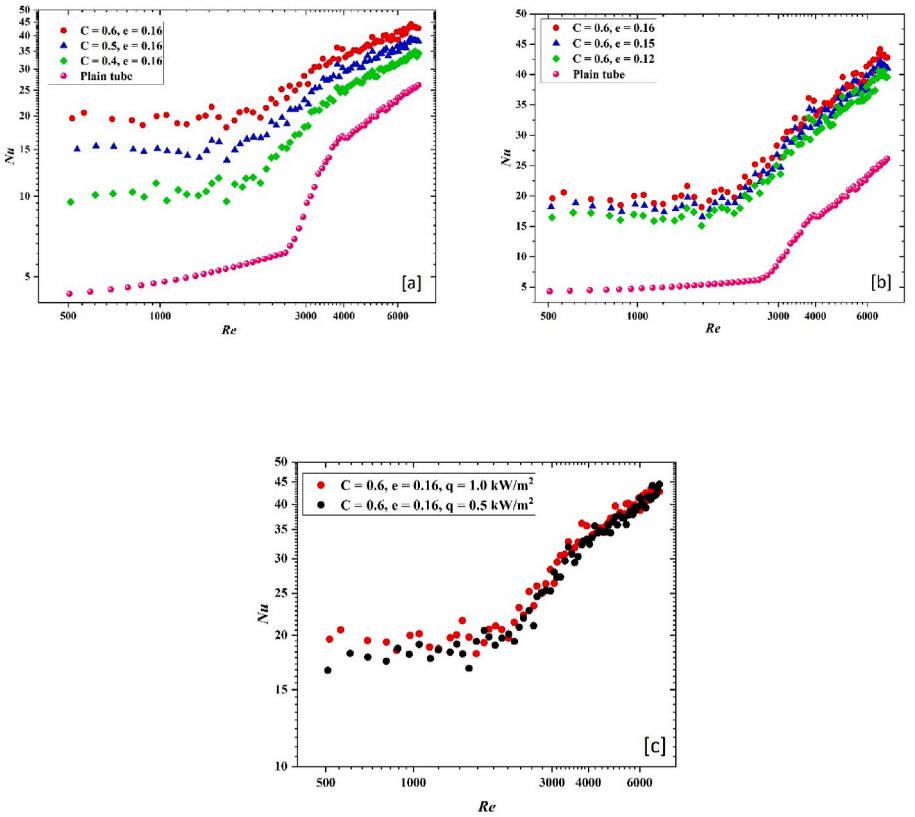

Fig. 3. Nusselt number as a function of Reynolds number: (a) at constant C = 0.6 and q = 1.0 kW/m^2, (b) at constant e = 0.16 and q = 0.5 kW/m^2, and (c) at different heat fluxes.

the friction factor as a function of Reynolds number.

Fig. 4 (a) shows the variation of friction factor with Reynolds number for constant clearance ratio (C = 0.6), and variable pitch ratio (e = 0.12, 0.15, 0.16) at 1 kW/m^2 heat flux. Following observations has been made from the figure:

(i) A sharp decrease in the friction factor has been reported in laminar flow regime with increase in the Reynolds number. In transitional flow regime, the friction factor again increases. However, on entering the turbulent flow regime, a slight but gradual decrease in the friction factor was observed.
(ii) A very slight variation in the friction factor value has been observed for all the configurations. However, on comparison to the plain channel the enhancement in the friction factor is appreciable.

Fig. 4 (b) shows the variation of friction factor for constant pitch ratio (e = 0.16) and variable clearance ratio (C = 0.4, 0.5, and 0.6) at heat flux of 1 kW/m^2. Following inferences has been made by observing the figure:

(i) Clearance ratio has significant influence on the friction factor. The difference can be clearly visible if we compare the results with Fig. 4 (a).
(ii) Decreasing trend has been observed for the friction factor in the laminar and turbulent flow regime while for the transition flow regime, friction factor shows increasing trend.
(iii) For the case of C = 0.6 and e = 0.16, the friction factor is highest followed by the friction factor for C = 0.5 and e = 0.16 and C = 0.4 and e = 0.16. This can be interpreted as pitch ratio of ribs do not show huge impact on the friction factor. However, if we consider the clearance ratio, the influence is visible and appreciable.

Fig. 4 (c) shows the variation of friction factor for C = 0.6 and e = 0.16, for different heat flux. It is visible from the figure that for higher heat flux the friction factor is higher while for lower heat flux value the friction factor is lower. The reason for higher friction factor is the interaction between the fluid particles. At higher heat flux, the fluid particles interact more with each other. This will cause the higher flow resistance and because of which higher friction factor and pressure drop.

The relationship between heat transfer and pressure drop is also revealed in term of ratio of friction factor to the Colburn j-factor (*f/j*). Fig. 5 (a and b) shows the variation of ratio *f/j* as a function of Reynolds number. Fig. 5 (a) shows the variation of *f/j* as a function of Reynolds number for constant clearance ratio (C = 0.6) while Fig. 5 (b) shows the variation of *f/j* for different heat flux conditions for C = 0.6 and e = 0.16. For C = 0.6 and e = 0.12, the *f/j* is highest while for C = 0.6 and e = 0.16, the *f/j* factor is lowest for constant heat flux of 1 kW/m^2. As far as Fig. 5 (b) is concerned no significant variation is observed.

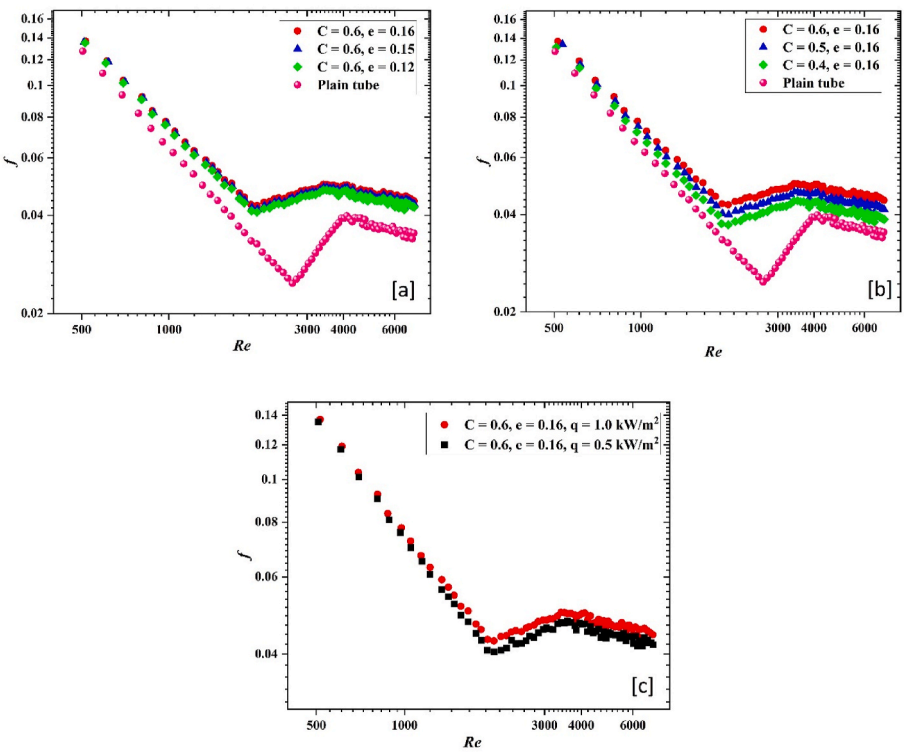

Fig. 4. Friction factor as a function of Reynolds number: (a) at constant C = 0.6 and q = 1.0 kW/m^2, (b) at constant e = 0.16 and q = 0.5 kW/m^2, and (c) at different heat fluxes.

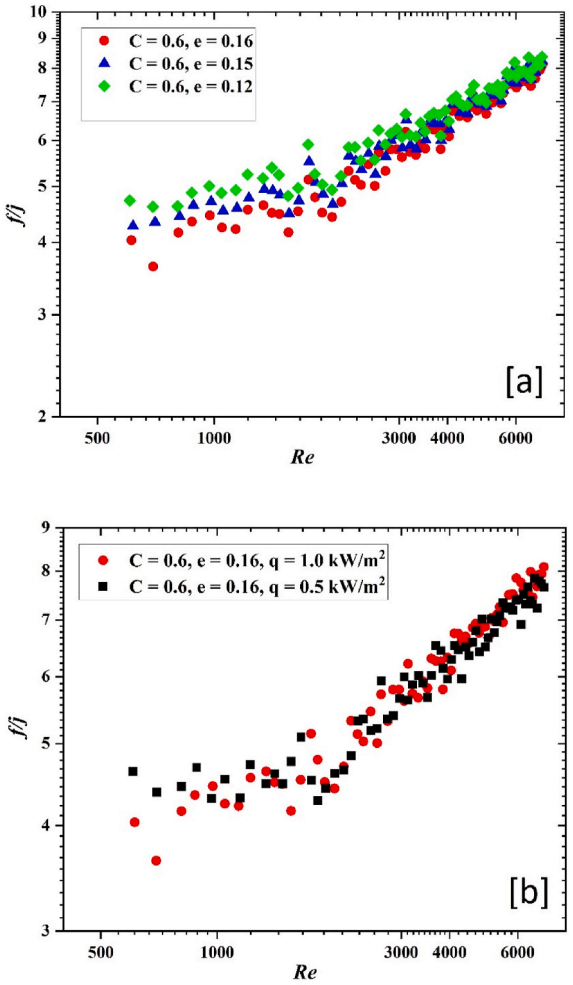

Fig. 5. f/j as a function of Re: (a) at constant = 1.0 kW/m^2, and (b) at different heat fluxes.

6.2.1. *Thermohydraulic performance factor (η)*

Thermohydraulic performance factor also known as thermal performance factor provides the performance of the heat exchangers by balancing the heat transfer enhancement with pressure drop. A design of heat exchanger is considered good if its value is more than unity. Fig. 6 shows the variation of η with Reynolds number. For the studied configurations, the value of η is more than unity. The highest value was reported for the case of C = 0.6 and e = 0.16 while the lowest values are reported for C = 0.4 and e = 0.12. A significant enhancement in the thermohydraulic performance factor was noticed upto the Reynolds number 3000. Beyond theoretical transition range, a sharp decrease in the value of thermal performance factor is observed.

Table 3 shows the comparison of various results in tabular format for easy and better understanding:

6.2.2. *Correlations*

The following novel correlations were developed from the experimental study for different flow regimes:

Nu for Re 500-4000

$$Nu = 0.7421 \times (0.5485 + 0.0114 \times Re) \times (1.3256–0.182 \times C+ 0.0021 \times e) \times q^{0.0456}$$

f for Re 500-4000

$$f = 1.9874 \times Re^{-0.111} \times (0.2214–0.0225 \times k + 0.00174 \times e) \times q^{0.0121}$$

Predicted outcomes from the novel correlations presented in Fig. 7. From the figure one can see that the error is minimum between experimental data and predicted points of *Nu* and *f*. The deviation of *Nu* is ±5% and f is ±6%.

7. Conclusions

In present experimental investigation, constant heat flux forced convection heat transfer and pressure drop inside a circular channel

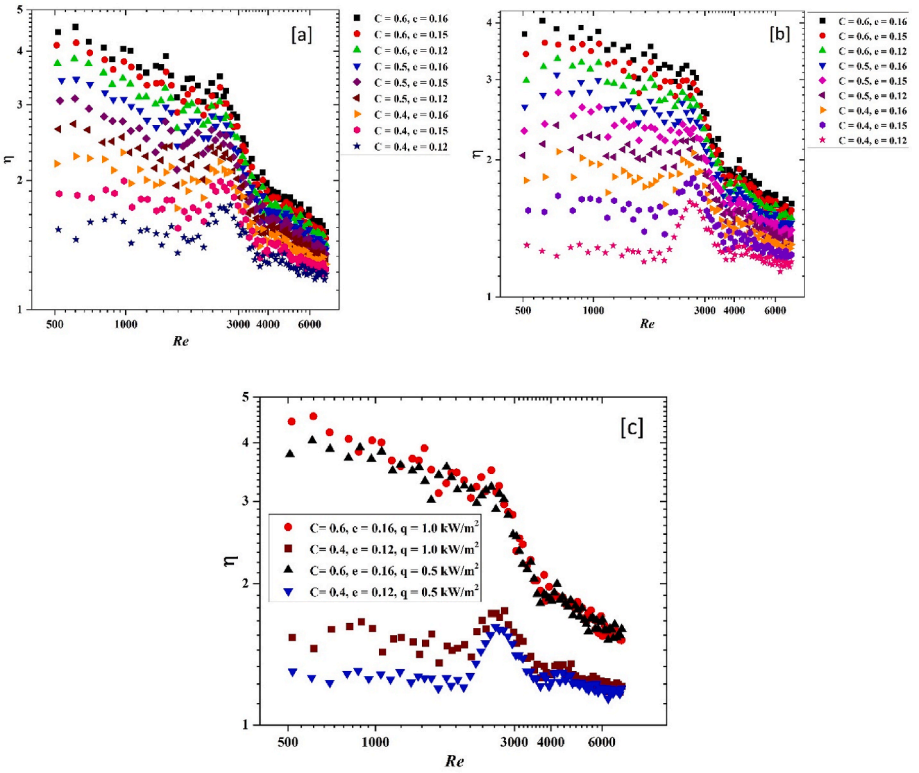

Fig. 6. Thermohydraulic performance factor as a function of Reynolds number: (a) at constant q = 1.0 kW/m^2, (b) at constant q = 0.5 kW/m^2, and (c) at different heat fluxes.

Table 3
Variation of Nu and *f* with various parameters for 1 and 0.5 kW-m^{-2} heat flux.

Heat flux (q)	Reynolds Number (Re)	Pitch ratio (e)	Clearance ratio (C)	Nu	*f*
1	1920	0.16	0.6	**21.033**	**0.04321**
1	1927	0.12	0.6	**18.11**	**0.04132**
1	1924	0.16	0.5	**16.404**	**0.04034**
1	1924	0.12	0.5	**12.322**	**0.03845**
1	1910	0.16	0.4	**11.685**	**0.03746**
1	1916	0.12	0.4	**8.323**	**0.03557**
0.5	1911	0.16	0.6	**18.978**	**0.04084**
0.5	1918	0.12	0.6	**15.8576**	**0.03895**
0.5	1915	0.16	0.5	**14.6901**	**0.03801**
0.5	1916	0.12	0.5	**11.9148**	**0.03602**
0.5	1930	0.16	0.4	**10.4621**	**0.03504**
0.5	1916	0.12	0.4	**7.0039**	**0.03409**

fitted with ribbed prism is investigated in laminar, transition and turbulent flow regime. Air is used as the working fluid with Reynolds number varied from 500 to 7036. The test section is heated with uniform heat flux of 0.5 and 1 kW/m^2. For plain channel heated with uniform heat flux of 1 kW/m^2, the transition begins at Re = 2562 and ends at Re = 3802. This brings the transition width of Re = 1240. When prism is placed in the channel, the boundaries of transition regime shifted significantly. As observed at 1 kW/m2 heat flux, for the case of C = 0.6 and e = 0.16, the transition begins at Re = 1648 and ends at Re = 3387 while for same case at 0.5 kW/m^2 heat flux, the transition begins at Re = 1554 and ends at Re = 3321. Highest enhancement in Nusselt number was reported for C = 0.6 and e = 0.16 while lowest enhancement was reported for C = 0.6 and e = 0.12 for channel having ribbed prism. Clearance ratio has significant influence on the friction factor. For the case of C = 0.6 and e = 0.16, the friction factor is highest followed by the friction factor for C = 0.5 and e = 0.16 and C = 0.4 and e = 0.16. A significant enhancement in the thermohydraulic performance factor was noticed upto the Reynolds number 3000. However, for all the cases the thermohydraulic performance factor remains greater than unity.

8. Future direction

As compared to laminar and turbulent flow regime, transition flow regime is fairly new and unexplored. Only few manuscripts are

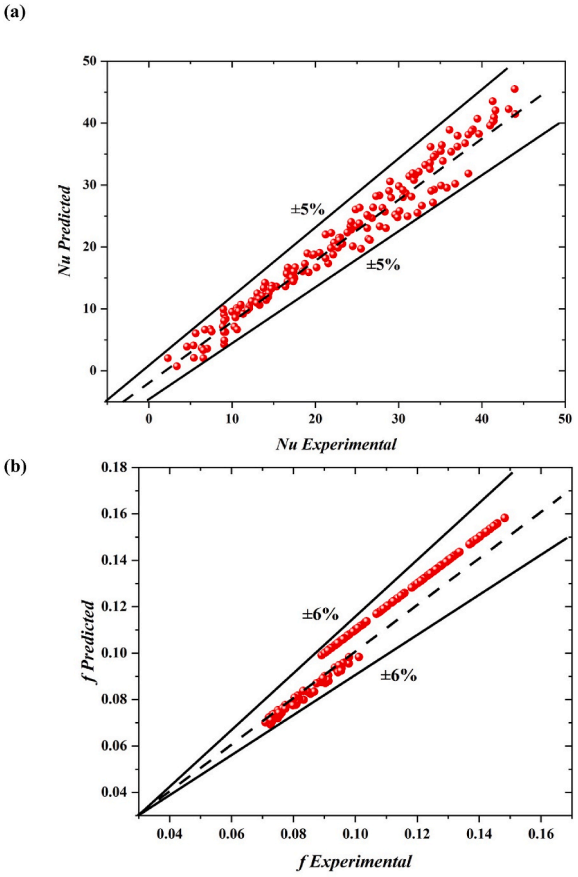

Fig. 7. Predicted data versus experimental data: (a) Nu, and (b) f.

available in the open literature with addresses the thermohydraulic characteristics of fluids in the transition flow regime. Furthermore, while the transitional flow regime's limits have been specified in the literature, they were qualitative and based on subjective visual observations. From the previous investigations on heat transfer and fluid flow in transition flow regime, it has been concluded that boundaries of transition flow regime are very wide, and it depends upon the different parameters such as inlet geometry, angle of inclination of test section, type of turbulators, working fluid, heat flux, etc. Amongst various studies of transition flow regime, fewer addresses on the influence of turbulators on the thermal and flow performance. Also, transition flow in microchannel remains untouched till date, as per the authors best knowledge and need attention.

Author statement

Assoc. Prof. Dr. Basma Souayeh: Conceptualization, Methodology, Validation, Investigation, Resources, Data Curation, Writing-Original Draft, Writing - Review & Editing, Visualization, Supervision. Dr. Suvanjan Bhattacharya: Conceptualization, Methodology, Writing- Original Draft, Writing- Review & Editing, Visualization, Supervision. Dr. Najib Hdhiri: Conceptualization, Methodology, Validation, Data Curation, Writing - Review & Editing. Dr. Mir Waqas Alam: Conducting a research and investigation process. Dr. Essam Yasin: Investigation, mathematical, computational. Dr. Muhammad Aamir: Writing - Review & Editing.

Declaration of competing interest

The authors declare that they have no known competing financial interests or personal relationships that could have appeared to influence the work reported in this paper.

Acknowledgments

This work was supported through the Annual Funding track by the Deanship of Scientific Research, Vice Presidency for Graduate Studies and Scientific Research, King Faisal University, Saudi Arabia [**Project No. AN00058**].

Nomenclature

Symbols

A_{Sur}	Surface area of channel
C_p	Specific heat
D	Internal diameter of plain channel
f	Friction factor
GI	Galvanized iron
h	average heat transfer coefficient
I	Current
j	Colburn j-factor
k	Spring ratio
k	Thermal conductivity
L	Length of channel
LR	Laminar regime
$m^{'}$	Mass flow rate
Nu	Nusselt number
P	Pitch of spring tape
Pr	Prandtl number
Q	Heat
q	Heat flux
Re	Reynolds number
$Re_{CR,C}$	Critical Reynolds number at completion of transition
$Re_{CR,S}$	Critical Reynolds number at start of transition
Re_{TFR}	Length of transition regime
T_b	Bulk temperature
TFR	Transition flow regime
T_{in}	Inlet temperature
T_{out}	Outlet temperature
TR	Turbulent regime
T_s	Surface temperature
T_{sx}	mean surface temperature at position x
$T(x)$	Local temperature at location x
T_x	mean temperature of working fluid at position x
V	Voltage

Greek

ρ	Density of fluid
μ	Dynamic viscosity of fluid
η	Thermal performance factor

Subscripts

0	plain channel

References

[1] N.A. Gatsonis, W.G. Al-Kouz, R.E. Chamberlin, Investigation of rarefied supersonic flows into rectangular nanochannels using a three-dimensional direct simulation Monte Carlo method, Phys. Fluids 22 (2010), 032001, https://doi.org/10.1063/1.3302805.

[2] S. Bhattacharyya, A.C. Benim, H. Chattopadhyay, A. Banerjee, Experimental and numerical analysis of forced convection in a twisted tube, Therm. Sci. 23 (2019) 1043–1052, https://doi.org/10.2298/TSCI19S4043B.

[3] S. Bhattacharyya, D. Sarkar, U.S. Mahabaleshwar, M.K. Soni, M. Mohanraj, Experimental study of thermohydraulic characteristics and irreversibility analysis of novel axial corrugated tube with spring tape inserts, EPJ Appl. Phys. 92 (2020) 30901, https://doi.org/10.1051/epjap/2020200192.

[4] S. Bhattacharyya, Fluid flow and heat transfer in a heat exchanger channel with short-length twisted tape turbulator inserts, Iran, J. Sci. Technol. - Trans. Mech. Eng. 44 (2020) 217–227, https://doi.org/10.1007/s40997-018-0251-0.

[5] S. Bhattacharyya, D.K. Vishwakarma, M.K. Soni, Heat transfer and pressure drop in transitional flow: a short review, IOP Conf. Ser. Mater. Sci. Eng. 1080 (2021), 012050, https://doi.org/10.1088/1757-899x/1080/1/012050.

[6] S. Bhattacharyya, D.K. Vishwakarma, V. Goel, S. Chamoli, A. Issakhov, J.P. Meyer, Thermodynamics and heat transfer study of a circular tube embedded with novel perforated angular-cut alternate segmental baffles, J. Therm. Anal. Calorim. 145 (2021) 1445–1465, https://doi.org/10.1007/s10973-021-10718-1.

[7] S. Bhattacharyya, D.K. Vishwakarma, S. Chakraborty, R. Roy, A. Issakhov, M. Sharifpur, Turbulent flow heat transfer through a circular tube with novel hybrid grooved tape inserts: thermohydraulic analysis and prediction by applying machine learning model, Sustainability 13 (2021) 3068, https://doi.org/10.3390/su13063068.

[8] S. Bhattacharyya, D.K. Vishwakarma, S. Roy, R. Biswas, M. Moghimi Ardekani, Applications of heat transfer enhancement techniques: a state-of-the-art review, IntechOpen, in: Inverse Heat Conduct. Heat Exch., 2020, https://doi.org/10.5772/intechopen.92873.
[9] A.J. Ghajar, K.F. Madon, Pressure drop measurements in the transition region for a circular tube with three different inlet configurations, Exp. Therm. Fluid Sci. 5 (1992) 129–135, https://doi.org/10.1016/0894-1777(92)90062-A.
[10] L.M. Tam, A.J. Ghajar, Effect of inlet geometry and heating on the fully developed friction factor in the transition region of a horizontal tube, Exp. Therm. Fluid Sci. 15 (1997) 52–64, https://doi.org/10.1016/S0894-1777(97)00035-6.
[11] A.J. Ghajar, C.C. Tang, Heat transfer measurements, flow pattern maps, and flow visualization for non-boiling two-phase flow in horizontal and slightly inclined pipe, Heat Tran. Eng. 28 (2007) 525–540, https://doi.org/10.1080/01457630701193906.
[12] H.K. Tam, L.M. Tam, A.J. Ghajar, Experimental analysis of the single-phase heat transfer and friction factor inside the horizontal internally micro-fin tube, in: ASME/JSME 2011 8th Therm, Eng. Jt. Conf., ASMEDC, 2011, pp. 44–48, https://doi.org/10.1115/AJTEC2011-44555.
[13] A.J. Ghajar, L.-M. Tam, Heat transfer measurements and correlations in the transition region for a circular tube with three different inlet configurations, Exp. Therm. Fluid Sci. 8 (1994) 79–90, https://doi.org/10.1016/0894-1777(94)90075-2.
[14] A.J. Ghajar, L.M. Tam, S.C. Tam, Improved heat transfer correlation in the transition region for a circular tube with three inlet configurations using artificial neural networks, Heat Tran. Eng. 25 (2004) 30–40, https://doi.org/10.1080/01457630490276097.
[15] A.J. Ghajar, L.M. Tam, Heat transfer measurements and correlations in the transition region for a circular tube with three different inlet configurations, Exp. Therm. Fluid Sci. 8 (1994) 79–90, https://doi.org/10.1016/0894-1777(94)90075-2.
[16] H.K. Tam, L.M. Tam, A.J. Ghajar, Effect of inlet geometries and heating on the entrance and fully-developed friction factors in the laminar and transition regions of a horizontal tube, Exp. Therm. Fluid Sci. 44 (2013) 680–696, https://doi.org/10.1016/j.expthermflusci.2012.09.008.
[17] A.J. Ghajar, Heat transfer and pressure drop in the transition region of smooth horizontal circular tubes with different inlet configurations, in: Adv. Heat Transf., Elsevier Ltd, 2019, pp. 1–53, https://doi.org/10.1016/bs.aiht.2019.05.001.
[18] J.P. Meyer, A.I. Bashir, M. Everts, Single-phase mixed convective heat transfer and pressure drop in the laminar and transitional flow regimes in smooth inclined tubes heated at a constant heat flux, Exp. Therm. Fluid Sci. 109 (2019), 109890, https://doi.org/10.1016/j.expthermflusci.2019.109890.
[19] J.P. Meyer, J.A. Olivier, Transitional flow inside enhanced tubes for fully developed and developing flow with different types of inlet disturbances: Part I – adiabatic pressure drops, Int. J. Heat Mass Tran. 54 (2011) 1587–1597, https://doi.org/10.1016/j.ijheatmasstransfer.2010.11.027.
[20] J.P. Meyer, J.A. Olivier, Transitional flow inside enhanced tubes for fully developed and developing flow with different types of inlet disturbances: Part II–heat transfer, Int. J. Heat Mass Tran. 54 (2011) 1598–1607, https://doi.org/10.1016/j.ijheatmasstransfer.2010.11.026.
[21] S.M. Abolarin, M. Everts, J.P. Meyer, The influence of peripheral u-cut twisted tapes and ring inserts on the heat transfer and pressure drop characteristics in the transitional flow regime, Int. J. Heat Mass Tran. 132 (2019) 970–984, https://doi.org/10.1016/j.ijheatmasstransfer.2018.12.051.
[22] J.P. Meyer, S.M. Abolarin, Heat transfer and pressure drop in the transitional flow regime for a smooth circular tube with twisted tape inserts and a square-edged inlet, Int. J. Heat Mass Tran. 117 (2018) 11–29, https://doi.org/10.1016/j.ijheatmasstransfer.2017.09.103.
[23] S.M. Abolarin, M. Everts, J.P. Meyer, Heat transfer and pressure drop characteristics of alternating clockwise and counter clockwise twisted tape inserts in the transitional flow regime, Int. J. Heat Mass Tran. 133 (2019) 203–217, https://doi.org/10.1016/j.ijheatmasstransfer.2018.12.107.
[24] P.F. Dunn, Measurement and Data Analysis for Engineering and Science, 2014, https://doi.org/10.1201/b16918.
[25] Y.A. Çengel, Heat and Mass Transfer : Fundamentals & Applications/Yunus A. Çengel, Afshin J. Ghajar, 2015.
[26] J.P. Meyer, M. Everts, Single-phase mixed convection of developing and fully developed flow in smooth horizontal circular tubes in the laminar and transitional flow regimes, Int. J. Heat Mass Tran. 117 (2018) 1251–1273, https://doi.org/10.1016/j.ijheatmasstransfer.2017.10.070.
[27] A.I. Bashir, M. Everts, R. Bennacer, J.P. Meyer, Single-phase forced convection heat transfer and pressure drop in circular tubes in the laminar and transitional flow regimes, Exp. Therm. Fluid Sci. 109 (2019), 109891, https://doi.org/10.1016/j.expthermflusci.2019.109891.
[28] Y.A. Çengel, J.M. Cimbala, Fluid Mechanics A Fundamental Approach, 2018.
[29] S. Bhattacharyya, D.K. Vishwakarma, A. Srinivasan, M.K. Soni, V. Goel, M. Sharifpur, M.H. Ahmadi, A. Issakhov, J. Meyer, Thermal performance enhancement in heat exchangers using active and passive techniques: a detailed review, J. Therm. Anal. Calorim. (2022), https://doi.org/10.1007/s10973-021-11168-5.